



High-pressure phase transformations of FeS: Novel phases at conditions of planetary cores

Shigeaki Ono^{a,b,*}, Artem R. Oganov^{c,d}, John P. Brodholt^a, Lidunka Vočadlo^a, Ian G. Wood^a, Andriy Lyakhov^c, Colin W. Glass^c, Alexander S. Côté^a, G. David Price^a

^a Department of Earth Sciences, University College London, Gower Street, London WC1E 6BT, UK

^b Institute for Research on Earth Evolution, Japan Agency for Marine–Earth Science and Technology, 2-15 Natsushima-cho, Yokosuka-shi, Kanagawa 237-0061, Japan

^c Laboratory of Crystallography, Department of Materials, ETH Zurich, Wolfgang-Pauli-Str. 10, CH-8093 Zurich, Switzerland

^d Geology Department, Moscow State University, 119992 Moscow, Russia

ARTICLE INFO

Article history:

Received 13 July 2007

Received in revised form 8 May 2008

Accepted 9 May 2008

Available online 27 May 2008

Editor: R.W. Carlson

Keywords:

iron sulfide

phase transformation

magnetic property

high pressure

first principles calculation

evolutionary crystal structure prediction

ABSTRACT

Iron sulfide (FeS) was investigated using first-principles calculations up to a pressure of 400 GPa. A number of new phase transitions were found. An antiferromagnetic MnP-type structure, FeS II, was confirmed to be stable at low pressures, whereas at high pressures (40–135 GPa) we find a new stable phase, with a non-magnetic MnP-type structure, FeS VI. The observed first-order change in the cell shape between the two phases can be explained by the difference in magnetic configurations. The calculated cell parameters, atomic coordinates, and bulk modulus of non-magnetic MnP-type phase are consistent with those determined from experiment. The upper pressure limit of the stability of the non-magnetic MnP-type phase was calculated to be 135 GPa. A hitherto unsuspected phase transition from the non-magnetic MnP-type to a phase with *Pmnn* symmetry, FeS VII, was identified using the evolutionary crystal structure prediction (USPEX) method. The structure of the *Pmnn* phase has no known analogues, but can be described as a distortion of the NaCl-type structure. The *Pmnn* phase with the distorted NaCl-type structure is stable from 135 GPa at least up to 400 GPa. According to previous experiments and the present study, the transition sequence of FeS at low temperatures is as follows: troilite → antiferromagnetic MnP-type phase → monoclinic phase → non-magnetic MnP-type phase → *Pmnn* phase. The calculated volume reduction from the monoclinic to the non-magnetic MnP-type phase is 1.0% at 40 GPa, which is in good agreement with experimental observations. The calculated volume reduction from the non-magnetic MnP-type to the *Pmnn* phase is 3.7% at 135 GPa.

© 2008 Elsevier B.V. All rights reserved.

1. Introduction

The Earth's core is believed to be less dense than pure iron at pressures and temperatures corresponding to core conditions, implying the presence of a substantial amount of dissolved light elements (e.g., Birch, 1952; Dewaele et al., 2006). Most of these light elements might have been incorporated into the core through a process of core-mantle segregation by the reaction between molten iron and silicate melt in early Earth history. According to cosmochemical arguments, candidates for the light elements include sulfur, silicon, oxygen, hydrogen, and carbon. Thus, in order to understand the composition of the Earth's core, it is important to clarify the phase relations of iron alloys at high pressures and high temperatures. Sulfur is likely to be one of the major light elements in the cores of planets such as Earth

and Mars (Dreibus and Palme, 1996; Allègre et al., 2001), and we therefore concentrate on this light element in this study.

The high-pressure behaviour of iron sulfide (FeS) has been investigated by both high-pressure experiments and *ab initio* simulations in many previous studies (King and Prewitt, 1982; Sherman, 1995; Fei et al., 1995; Kusaba et al., 1997; Kobayashi et al., 1997; Alfè and Gillan, 1998; Kusaba et al., 1998; Nelmes et al., 1999; Takele and Hearne, 1999; Rueff et al., 1999; Vočadlo et al., 2000; Marshall et al., 2000; Kavner et al., 2001; Martin et al., 2001; Urakawa et al., 2004; Kobayashi et al., 2004; Ono and Kikegawa, 2006). Antiferromagnetic troilite (FeS I) is the stable phase at ambient conditions. The structure of troilite with space group *P*-62c is close to that of NiAs-type structure. With increasing pressure, a structural transition from troilite to the MnP-type structure (FeS II), which is also antiferromagnetic, was observed at ~3.5 GPa (King and Prewitt, 1982; Takele and Hearne, 1999). This structure has space group *Pnma* and the orthorhombic cell dimensions $a=c$, $b=A$ and $c=\sqrt{3}A$, where A and C refer to cell parameters of an NiAs-type structure. The magnetic spin direction of this MnP-type phase is aligned along the *b* axis (Marshall et al., 2000). The next structural transition, accompanied by the

* Corresponding author. Present address: Institute for Research on Earth Evolution, Japan Agency for Marine–Earth Science and Technology, 2-15 Natsushima-cho, Yokosuka-shi, Kanagawa 237-0061, Japan. Tel.: +81 46 867 9762; fax: +81 46 867 9625.
E-mail address: sono@jamstec.go.jp (S. Ono).

disappearance of a magnetic moment, is to a monoclinic structure (FeS III) (King and Prewitt, 1982; Rueff et al., 1999; Takele and Hearne, 1999) at ~ 7 GPa. Recently, a new MnP-type phase (FeS VI) was confirmed, and the transition pressure between it and the monoclinic phase is 40 GPa (Ono and Kikegawa, 2006). Although the structure of this new phase (Ono and Kikegawa, 2006) is the same as that of the antiferromagnetic MnP-type phase (King and Prewitt, 1982), a large volume reduction and a significant difference in the ratios of cell parameters was observed between these two phases. It is possible that a pressure-induced collapse of magnetization occurs between the antiferromagnetic and the new MnP-type phase in FeS; for example, it has been observed that FeO exhibits a similar pressure-induced spin transition, which causes a volume reduction and change in cell parameters without any structural transition (Ono et al., 2007a). Using *ab initio* calculations, Martin et al. (2001) predicted that the monoclinic phase of FeS transforms to a CsCl-type phase and suggested that the CsCl-type phase is most likely to be stable at the Earth's inner core pressures. This view is supported by theoretical calculations and high-P experiments which show that the CsCl-type structure is stable at high pressures in other iron alloys, such as FeSi (Vočadlo et al., 1999; Dobson et al., 2002; Ono et al., 2007b). Martin et al. (2001) did not, however, perform calculations on the MnP-type phase recently discovered by Ono and Kikegawa (2006). Although the experiments of Ono and Kikegawa (2006) show the MnP phase to be stable to at least 120 GPa, whether it remained stable under the Earth's inner core conditions was unknown.

In this study, we carried out *ab initio* calculations to investigate the magnetic properties of the newly discovered MnP-type phase within the framework of density functional theory. The collapse of magnetization between the antiferromagnetic and new MnP-type phase was clearly identified. Furthermore, we also used the recently developed evolutionary crystal structure prediction methodology (Oganov et al., 2006; Oganov and Glass, 2006; Glass et al., 2006), which has resulted in the prediction of another new phase stable at least up to 400 GPa at 0 K.

2. Computational methodology

2.1. Static structure relaxations and enthalpy calculations

First-principles calculations performed in this study were based on density functional theory (DFT) within the generalized gradient approximation (GGA) (Wang and Perdew, 1991). The electronic wave functions are expanded in a plane-wave basis set with a cutoff energy of 600 eV, and the electron-ion interaction is described by means of the projector augmented wave (PAW) method (Blöchl, 1994; Kresse and Joubert, 1999) as implemented in the Vienna *ab initio* simulation package (VASP) (Kresse and Furthmüller 1996). The accuracy of this method for FeS has been checked in previous studies (Alfè and Gillan, 1998; Vočadlo et al., 2000). All electronic states up to 3p and 2p are treated as frozen core states with a [Ne]3 s^2 core for Fe and with a [Ne] core for S. Integration over the Brillouin zone was performed using a Monkhorst–Pack grid, with the number of k-points ranging from 4–286 depending on the cell size and shape. The Methfessel–Paxton (Methfessel and Paxton, 1989) electronic smearing method, with the smearing width of 0.2 eV, was used to improve convergence of the energies/forces during structural optimization; final enthalpy calculations were done on the relaxed structures. The equilibrium structure was obtained after a full geometry optimization using the conjugate gradients method. The total energies, except for troilite, were converged to within 1 meV per atom (calculations for troilite are ~ 5 meV). Suitable super-cells were used in the calculations of antiferromagnetic phases (for both troilite and the MnP-type phase); the spin configurations of the antiferromagnetic phases used in this study were the same as those reported in Martin et al. (2001). For the correlation energy of spin-polarised systems we used the spin-in-

terpolation formula of (Vosko et al., 1980). A comprehensive review of this methodology has been given elsewhere (Gillan et al., 2006).

2.2. Evolutionary crystal structure prediction

To find the stable high-pressure structures of FeS, we have performed simulations based on the evolutionary algorithm USPEX, developed by our previous studies (Oganov et al., 2006; Oganov and Glass, 2006; Glass et al., 2006). An exhaustive description of the method was given in the above references, to which we redirect the reader for details. Structure relaxations and enthalpy calculations, the underlying evolutionary search in the USPEX code, were performed using the VASP code (Kresse and Furthmüller, 1996), using computational conditions similar to those described in the previous section. The differences are minor and include the use of a different GGA formulation (Perdew et al., 1996), lower plane-wave energy cut-off of 370 eV (which already gives very good convergence), automatically generated k -point meshes with a constant reciprocal-space resolution of 0.09 \AA^{-1} (at 400 GPa we used a resolution of 0.07 \AA^{-1}) and a smaller smearing width of 0.1 eV. The Kohn–Sham equations were solved self-consistently with the threshold of 10^{-4} eV/cell and conjugate-gradients structure relaxations were performed until forces on the atoms were below 10^{-3} eV/Å. Two types of evolutionary simulations were performed: (i) a fixed-cell run at experimental cell parameters corresponding to 56 GPa from Ono and Kikegawa (2006), with 8 atoms/cell, (ii) constant-pressure variable-cell runs at 56 GPa, 120 GPa and 400 GPa. The following system sizes were considered in variable-cell simulations: 4, 6, 8, 12, and 16 atoms/cell. The populations included 20–50 structures for systems with 4–16 atoms/cell, and the first generation was always produced randomly. All the newly produced structures were relaxed and ranked by their enthalpy values. The highest-enthalpy 40% of the population were discarded and from the remaining structures the next generation was produced using three variation operators (in variable-cell simulations, 70–80% of the child structures were produced through heredity, 0–10% using permutation, 20% by lattice mutation); in addition, the lowest-enthalpy structure of the previous generation survived into the next generation. The Gaussian strength of lattice mutation (Oganov and Glass, 2006) was 0.55 and in permutation atomic swaps were performed on up to 2 pairs of different atoms. Simulations were terminated when no improvement of the best structure was found for more than 10–20 generations (for systems with 4–16 atoms/cell).

3. Results and discussion

3.1. Rietveld refinement

As the precise cell parameters and atomic coordinates are important for understanding the unique behaviour of the newly discovered MnP-type phase, we performed a Rietveld refinement of an X-ray diffraction pattern of this phase that had been obtained in a diamond anvil cell at 56 GPa and 300 K in a previous experimental study (Ono and Kikegawa, 2006). The new structure was initially solved by comparing the axial ratios given in Ono and Kikegawa (2006) with those of the various polymorphs of FeS considered by Martin et al. (2001); this indicated that the structure was likely to be an MnP-type phase and refinement on this basis, from starting coordinates taken from Martin et al. (2001), was successful. The MnP-type structure is orthorhombic ($Pnma$) with $Z=4$; the Fe atoms are coordinated by six S atoms arranged in an octahedron. As described above, the MnP-type structure of FeS is related to the NiAs-type cell, with hexagonal symmetry (King and Prewitt, 1982), and is a superstructure of the NiAs-type cell.

The Rietveld refinement was performed using the program GSAS (Larson and von Dreele, 2000; Toby, 2001). Two phases were considered, the MnP-type FeS and the CsCl-structured NaCl pressure

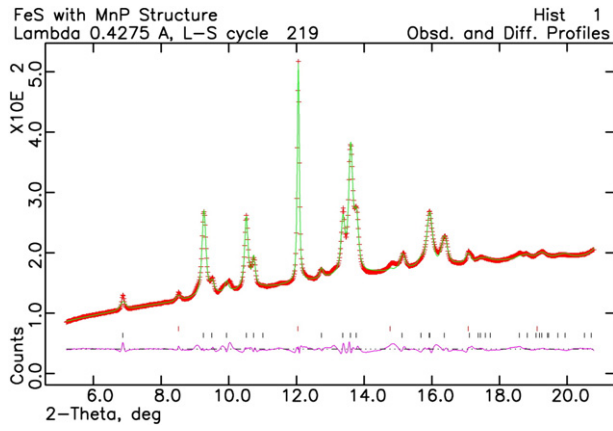


Fig. 1. Rietveld refinement of the X-ray diffraction pattern of the non-magnetic MnP-type phase (FeS VI) at 56 GPa and 300 K (data taken from Ono and Kikegawa, 2006). The observed diffraction pattern is shown as points and the calculated pattern as a continuous line; the lower trace gives the difference. The vertical bars mark the positions of the reflections from FeS (lower set) and NaCl (CScI phase) respectively.

calibrant; in total, 39 variables were included at various stages in the refinement: 4 positional parameters, 2 atomic displacement (thermal) parameters, 4 lattice parameters, 2 scale factors, the zero point, 8 profile coefficients (4 for each phase), 8 background coefficients (8-th order Chebyshev polynomial) and 10 preferred orientation coefficients (9 for FeS, 1 for NaCl). Because of the relatively limited d -spacing range and quality of the data, it was found that not all parameters could be varied simultaneously. Therefore, it was decided to use only a single isotropic displacement (thermal) parameter for each phase. Introduction of a preferred orientation correction for the FeS was found to greatly improve the quality of the fit; a 6-th order spherical harmonic correction was used, with the resulting texture index equal to 1.66 (a 4-th order correction applied to the NaCl, texture index=1.08, made only a marginal improvement). The final reduced χ^2 for 31 variables (with the profile coefficients not refined) was 0.044, with weighted and unweighted profile R -factors of 0.016 and 0.012 respectively. Fig. 1 shows the result of the Rietveld refinement; the refined structural parameters are given in Table 1.

3.2. *Ab initio* calculations

We calculated two spin configurations in the MnP-type phases. The antiferromagnetic configuration has already been calculated by Martin et al. (2001), and our results are in excellent agreement with their study (Table 2). Non-collinear calculations were performed to see how spin-orbit coupling was related to the direction of the magnetic moment of iron. As this has no influence on cell parameters and volume, the direction of the magnetic moment was not considered further in this study. We also calculated the non-magnetic configuration in the MnP-type phase. From the calculated enthalpies of both MnP-type phases, the antiferromagnetic state is stable at low pressures. The variation in the volumes of both antiferromagnetic and non-magnetic phases is shown in Fig. 2. The calculated volumes of the antiferromagnetic phase are slightly smaller than those inferred from

Table 1

Structural parameters resulting from Rietveld refinement of the non-magnetic MnP-type phase (FeS VI) at 56 GPa and 300 K

Cell parameters	a (Å)	b (Å)	c (Å)	V (Å ³)
	4.9371(9)	3.0844(6)	5.1576(11)	78.540(15)
Atom	Site	x	y	z
Fe	4c	0.0051(18)	1/4	0.2001(7)
S	4c	0.2085(18)	1/4	0.5800(18)

Space group: $Pnma$ ($Z=4$). *Values constrained to be equal. $R_{wp}=0.016$.

Table 2

Cell parameters and atomic coordinates of the antiferromagnetic and non-magnetic MnP-type phases

	AFM MnP			NM MnP	
	Exp. ^a	Cal. ^b	This study	Exp. ^c	This study
a	5.7449	5.685	5.592	4.937	4.892
b	3.3782	3.389	3.297	3.084	3.121
c	5.8048	5.780	5.695	5.158	5.143
V	112.65	111.36	105.00	78.53	78.52
c/a	1.010	1.017	1.018	1.045	1.051
Fe					
x	0.0117	0.014	0.0150	0.0051	0.0116
y	0.25	0.25	0.25	0.25	0.25
z	0.2038	0.192	0.1947	0.2001	0.2002
S					
x	0.223	0.218	0.2166	0.2085	0.2019
y	0.25	0.25	0.25	0.25	0.25
z	0.576	0.577	0.5736	0.5800	0.5871
P (GPa)	4	0	4	56	56
T (K)	Room temperature	0	0	Room temperature	0

Abbreviations are as follows: AFM MnP, antiferromagnetic MnP-type phase (FeS II); NM MnP, non-magnetic MnP-type phase (FeS VI). ^aMarshall et al. (2000). ^bMartin et al. (2001). ^cRietveld refinement of X-ray diffraction data from Ono and Kikegawa (2006).

experiments (Marshall et al., 2000). In contrast, the calculated volumes of the non-magnetic phase are in good agreement with experimental results (Ono and Kikegawa, 2006). The volume reduction of this magnetic transition was 7.1% at 7 GPa and 0 K. However, direct transition from the antiferromagnetic to the non-magnetic phase has not been observed in previous high-pressure experiments. According to previous experiments, the monoclinic phase is stable at pressures between the antiferromagnetic and the non-magnetic MnP-type phase stability fields.

Fig. 3 shows the effect of pressure on the unit cell parameters of both MnP-type phases. The c/a ratio of the antiferromagnetic phase is ~ 1 at ambient pressure. On the other hand, the c/a ratio of the non-magnetic phase is greater than 1 (Table 2). The value of the b axis of the antiferromagnetic phase is almost identical to that of the non-magnetic phase. However, significant differences in the c axis and, especially, in the a axis were observed between the two phases, which had also been identified by high-pressure experiments in previous studies (Marshall et al., 2000; Ono and Kikegawa, 2006). The different

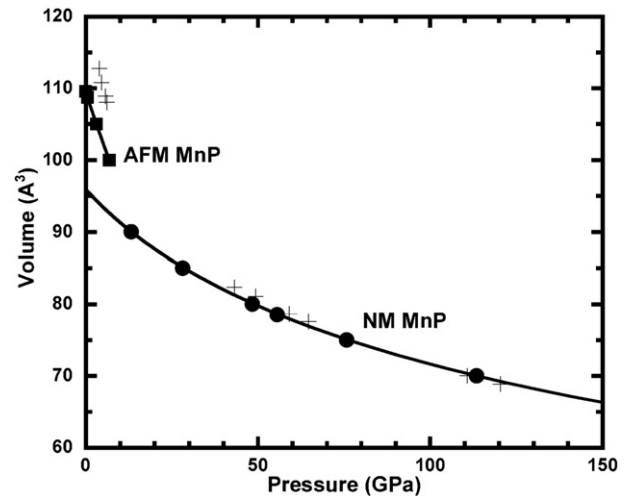


Fig. 2. Volume changes of antiferromagnetic (AFM) and non-magnetic (NM) MnP-type phases as a function of pressure at 0 K. Abbreviations of symbols are as follows: solid squares, AFM MnP-type phase (FeS II); solid circles, NM MnP-type phase (FeS VI); crosses, experimental data from Marshall et al. (2000) and Ono and Kikegawa (2006). Solid lines are the Birch–Murnaghan equation P – V fits for each phase calculated in this study.

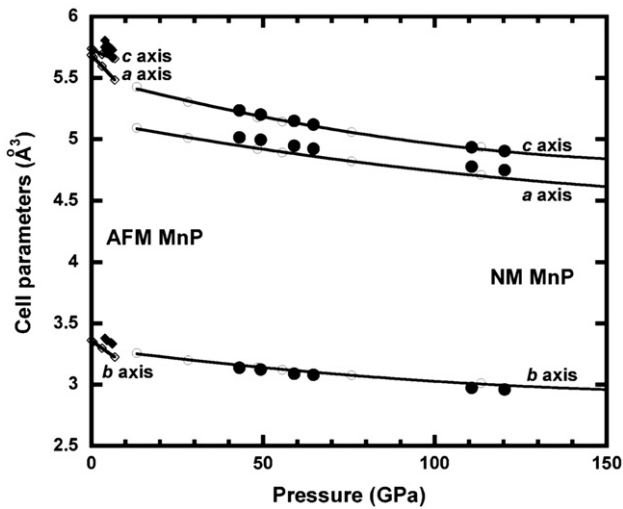


Fig. 3. Unit-cell parameters of antiferromagnetic (AFM) and non-magnetic (NM) MnP-type phases as a function of pressure at 0 K. Abbreviations of symbols are as follows: open diamonds, AFM MnP-type phase (FeS II); open circles, NM MnP-type phase (FeS VI); solid diamonds, experimental data (Marshall et al., 2000); solid circles, experimental data (Ono and Kikegawa, 2006). The solid lines are fits for each calculated cell parameter as a function of pressure.

magnetic configurations between the antiferromagnetic and the non-magnetic phases can reasonably explain this distortion. The atomic coordinates of both phases were also calculated in this study (Table 2). The results calculated in this study agree with those from high-pressure experiments and from previous calculations (Marshall et al., 2000; Martin et al., 2001; Ono and Kikegawa, 2006).

Next, we used the evolutionary algorithm USPEX (Oganov et al., 2006; Oganov and Glass, 2006; Glass et al., 2006) to investigate candidates for stable structure at extremely high pressure conditions. Evolutionary simulations with fixed experimental unit cell parameters (measured at 56 GPa) clearly yielded the non-magnetic MnP-type structure, *Pnma*. This supports the conclusion reached here using Rietveld refinement and static *ab initio* structure optimisations. In

Table 3
Comparison of the isothermal bulk modulus of FeS phases

K_0 (GPa)	K_0'	V_0 (Å ³)	Method
Troilite (FeS I), <i>P-62c</i>			
82	-5	723.84	Exp. (King and Prewitt, 1982)
73			Exp. (Kusaba et al., 1997)
75.6	-0.9	697.44	Cal. (Martin et al., 2001)
65.2	-1.28	682.80	Cal. (this study)
AFM MnP (FeS II), <i>Pnma</i>			
35	5	112.8	Exp. (King and Prewitt, 1982)
44		107.56	Exp. (Kusaba et al., 1997)
76.8	2.20	111.36	Cal. (Martin et al., 2001)
73.1	0.94	109.57	Cal. (this study)
Monoclinic (FeS III), <i>P2₁/a</i>			
96		290.04	Exp. (Kusaba et al., 1997)
127			Exp. (Kobayashi et al., 1997)
157.7	4.72	295.8	Cal. (Martin et al., 2001)
157.6	5.02	293.57	Cal. (this study)
NM MnP (FeS VI), <i>Pnma</i>			
156	4	99.5	Exp. (Ono and Kikegawa, 2006)
175.7	4.39	96.24	Cal. (this study)
<i>Pmnn</i> (FeS VII), <i>Pmnn</i>			
176.0	4.35	46.95	Cal. (this study)
Metastable NM-CsCl, <i>Pm-3 m</i>			
190	4.06		Cal. (Sherman, 1995)
191	4.11	22.99	Cal. (Alfè and Gillan, 1998)
173.7	4.55	23.18	Cal. (Martin et al., 2001)
172.5	4.54	23.15	Cal. (this study)

K_0 and K_0' are the isothermal bulk modulus and the first derivative of the isothermal bulk modulus, respectively.

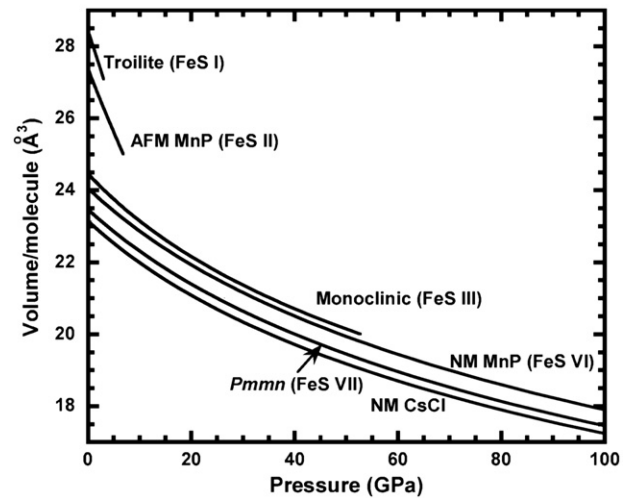


Fig. 4. Calculated volume change of different FeS phases as a function of pressure at 0 K. The lines denote the fitted curves for phases of troilite (FeS I), antiferromagnetic MnP-type (FeS II), monoclinic (FeS III), non-magnetic MnP-type (FeS VI), *Pmnn* (FeS VII), and non-magnetic CsCl-type.

variable-cell simulations at 56 GPa, the MnP-type structure is clearly the most stable one, whereas at 120 GPa it is only marginally more stable than a distorted NaCl-type structure, *Pmnn*, and at 400 GPa the *Pmnn* phase came up as being most stable. The *Pmnn* phase was unexpected and it belongs to a new structure type (i.e. no material with this structure is currently known). It can be best described as a distortion of the NaCl-type structure. It turns out to be more stable than the CsCl-type phase (which has often been postulated as stable at high pressure) at all conditions at least up to 400 GPa.

Finally, we also performed calculations using the conventional static structure relaxation method on the troilite phase, the monoclinic phase, the non-magnetic *Pmnn* phase, and the non-magnetic CsCl-type phase, in order to investigate the physical properties and the stability of these FeS phases. Table 3 shows the comparison of compressibility of the different FeS phases. The pressure-volume data were fitted to a third-order Birch–Murnaghan equation of state. There is a seemingly large discrepancy (e.g. for the bulk modulus) between experimental observations and calculations in the antiferromagnetic MnP-type phase. However, it is known that a wide range of pressure

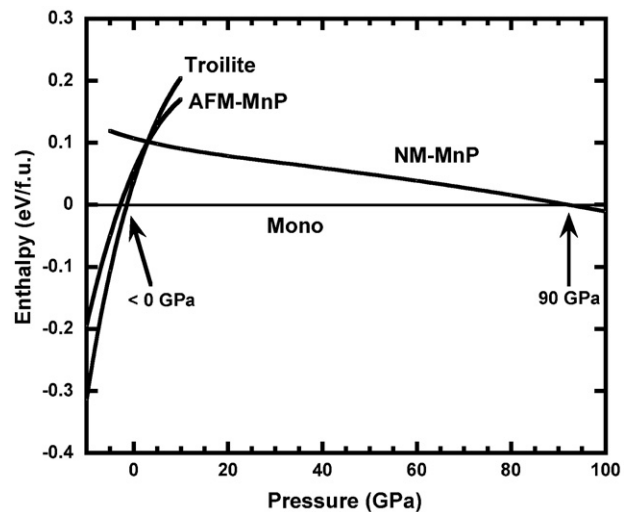


Fig. 5. Enthalpy differences of FeS phases. The solid lines denote the enthalpy differences of troilite, the antiferromagnetic MnP-type (AFM-MnP), and the non-magnetic MnP-type (NM-MnP) phases relative to the monoclinic (Mono) phase as function of pressure using the GGA formulation from Wang and Perdew (1991).

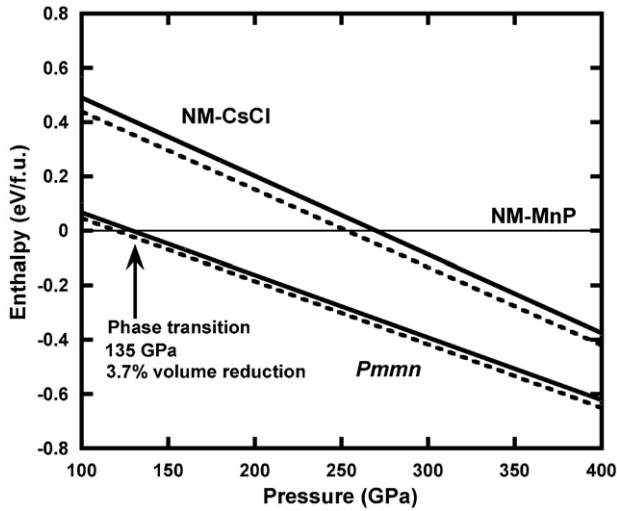


Fig. 6. Structural stability of $Pmmn$ FeS. The solid lines denote the enthalpy differences of the non-magnetic CsCl-type (NM-CsCl) and non-magnetic $Pmmn$ ($Pmmn$) phases relative to the non-magnetic MnP-type (NM-MnP) phase as function of pressure from calculations using the GGA formulation from Wang and Perdew (1991). The $Pmmn$ (distorted NaCl-type) phase is stable above 135 GPa. The dashed lines denote the enthalpy differences using the GGA formulation from Perdew et al. (1996).

data is needed to determine a reliable bulk modulus in high-pressure experiments, but the stability field of this phase is narrow (3–7 GPa), which precludes reliable fitting of the experimental equation of state. In contrast, the bulk modulus of the non-magnetic MnP-type phase calculated in this study is in good agreement with that measured by the previous high-pressure study (Ono and Kikegawa, 2006). As the $Pmmn$ phase predicted here has not yet been observed experimentally, we can only give the predicted properties. Our results on the metastable non-magnetic CsCl-type phase are consistent with those from previous calculations. Fig. 4 shows the change in volume of the FeS phases calculated in this study. At ~ 7 GPa and room temperature, the phase transition from the antiferromagnetic MnP-type to the monoclinic phase, accompanied by a $\sim 6\%$ volume reduction, was confirmed

Table 4

Structures of non-magnetic MnP-type and distorted NaCl-type phases optimized at 130 GPa

	NM MnP-type phase (FeS VI)			$Pmmn$ phase (FeS VII)		
Space group	$Pnma$			$Pmmn$		
a (Å)	4.6656			2.5059		
b (Å)	2.9871			3.8494		
c (Å)	4.8931			3.4401		
Atomic coordinates	x	y	z	x	y	Z
Fe	0.01510	0.25	0.19505	0	0.5	0.35783
S	0.19286	0.25	0.58763	0	0	0.14545
Interatomic distances (in Å, up to 2.7 Å)	Fe–S: 2.042 ($\times 1$), 2.074 ($\times 2$), 2.089 ($\times 2$), 2.092 ($\times 1$), Fe–Fe: 2.394 ($\times 2$), 2.428 ($\times 2$), S–S: 2.490 ($\times 2$).			Fe–S: 2.059 ($\times 2$), 2.119 ($\times 2$), 2.137 ($\times 2$), Fe–Fe: 2.496 ($\times 2$), 2.506 ($\times 2$), S–S: 2.5052 ($\times 4$), 2.506 ($\times 2$).		
Octahedron volume	11.366			11.061		
D	0.0063			0.0146		
$\langle \lambda \rangle$	1.0338			1.0814		
σ^2	114.01			318.05		

Octahedron volume is the volume of FeS_6 polyhedron in Å^3 . D , $\langle \lambda \rangle$, and σ^2 are the distortion index of bond length in the FeS_6 octahedron, the quadratic elongation of the FeS_6 octahedron, and the bond angle variance in the FeS_6 octahedron (deg^2), respectively. $D = \frac{1}{n} \sum_{i=1}^n \frac{l_i - l_{av}}{l_{av}}$, where n , l_i , and l_{av} are the coordination number of the Fe, the distance from the Fe to the i th coordinating S, and the average bond length, respectively. $\langle \lambda \rangle = \frac{1}{n} \sum_{i=1}^n \frac{l_i}{l_0}$, where n , l_i , and l_0 are the coordination number of Fe, the distance from Fe to the coordinating S, and the center-to-vertex distance of a regular octahedron of the same volume, respectively. $\sigma^2 = \frac{1}{m-1} \sum_{i=1}^m (\phi_i - 90) ^2$, where m and ϕ_i are 12 for the FeS_6 octahedron and the i th bond angle of S–Fe–S in the octahedron, respectively.

in a high-pressure study by Kusaba et al. (1997). Our calculations showed a 5.8% volume reduction at 7 GPa and 0 K for this transition. The next pressure-induced phase transition from the monoclinic to the non-magnetic MnP-type phase, accompanied by a $\sim 1\%$ volume reduction, was found experimentally to occur at ~ 40 GPa (Ono and Kikegawa, 2006). We also determined a 1.0% volume reduction for this transition at 40 GPa and 0 K, which is in excellent agreement with the experimental observations.

The enthalpies of each phase were calculated to investigate the transition pressures (Fig. 5). The enthalpy was obtained directly in our calculations as $H = E + PV$, where E is the internal energy. Although cell parameters and volumes of each phase from our calculations are in general agreement with those from experiments, our calculations could not predict transition pressures in quantitative agreement with experiment (King and Prewitt, 1982; Ono and Kikegawa, 2006). Troilite and the antiferromagnetic MnP-type phase were metastable in our calculations at all pressures between 0 GPa and 400 GPa (but stable at negative pressures, i.e. shifted downwards by several GPa relative to experiment). In contrast, the transition from the monoclinic to the non-magnetic MnP-type phase in our calculations occurs at ~ 90 GPa, which is significantly higher than experimental transition pressure of 40 GPa (Ono and Kikegawa, 2006; Ohfujii et al., 2007). Thus, GGA calculations overestimate the stability of the monoclinic phase. It is known that DFT fails to correctly describe some of the physical properties of FeO (e.g., Alfredsson et al., 2004). Although

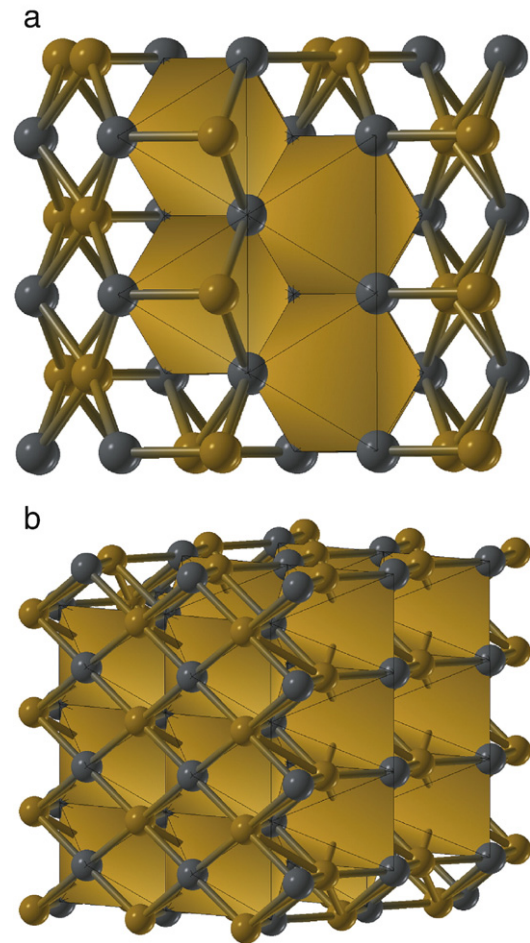


Fig. 7. Structures of high-pressure non-magnetic phases of FeS. a) non-magnetic MnP-type structure (FeS VI), $Pnma$; b) d-NaCl-type structure (FeS VII), $Pmmn$. The yellow and black spheres denote iron and sulfur atoms, respectively. The polyhedra denote FeS_6 octahedra. Structure visualizations were performed with the STM3 code (Valle, 2005).

some properties predicted by LDA calculations generally agree with experimental values (Isaak et al., 1993), FeO was predicted to be a metal at zero pressure within the LDA method. The LDA+*U* method, which allows treatment of correlated electrons with strong localized repulsions, is needed to obtain an insulating state of FeO at zero pressure (Gramsch et al., 2003). An influence of the on-site Coloumb repulsions was not considered in this study. In the case of our FeS calculations, the transition pressures calculated by DFT are likely to include a significant uncertainty; however, the density differences between the phases and sequences of phases with increasing pressure are correct. It is likely that the influence of the local Coloumb repulsions is important to obtain more reliable transition pressures in the FeS composition.

Fig. 6 shows the calculated static enthalpy difference between the non-magnetic MnP-type, the *Pmmn*, and the CsCl-type phases. The phase transition from the non-magnetic MnP-type to the non-magnetic *Pmmn* phase is predicted to occur at 135 GPa and 0 K. The exact value of the transition pressure depends on the exchange-correlation functional: as shown in Fig. 6, another GGA formulation (Perdew et al., 1996) gives the transition pressure of 127 GPa, i.e. ~10 GPa lower than the GGA functional of Wang and Perdew (1991). The calculated volume reduction at this transition is 3.7%. The non-magnetic CsCl-type phase turns out not to be stable in the pressure range explored here; our results indicate that the *Pmmn* phase is the most stable structure of FeS at the pressures of the Earth's core. The calculated structures of the non-magnetic MnP-type and the *Pmmn* phases at 130 GPa (i.e. near the phase transition) are given in Table 4 and Fig. 7. The distances of Fe–S, Fe–Fe, and S–S in the *Pmmn* phase are longer than those in the MnP-type phase. Although the Fe–S distances increase, the *Pmmn* phase is denser because of the larger distortion of the FeS₆ octahedron, which causes a decrease in the octahedron volume. The stability of the *Pmmn* phase may be explained by a denser packing with longer repulsive distances. The stability of the *Pmmn* phase may be explained by a denser close packing with longer bonding of repulsive ions. Tremel et al. (1986) have analyzed the nature of various distortions of the NiAs-type structure, tracing them to electronic stabilization due to Jahn–Teller-type distortions and electronic pseudogap formation. Among other things, they have noticed that the MnP-type distortion of the NiAs structure occurs when the number of valence electrons is 11–14 per formula. FeS, having 14 valence electrons, is therefore at the limit of stability of the MnP structure type and should be prone to phase transitions. The complicated phase diagram of FeS (Fig. 8) is consistent with this picture. Magnetism, not considered by Tremel et al. (1986), increases the complexity even further.

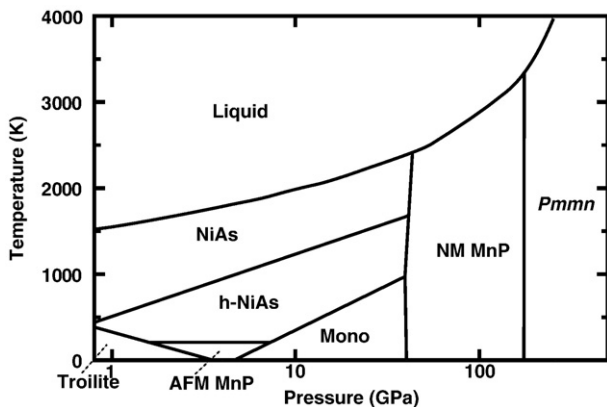


Fig. 8. Schematic phase diagram of FeS phases. Troilite (Fe I), *P*-*6*2c; AFM MnP (Fe II), antiferromagnetic MnP-type structure, *Pnma*; Mono (Fe III), monoclinic structure, *P2₁/a*; h-NiAs (Fe IV), hexagonal NiAs-type super-structure; NiAs (Fe V), simple NiAs-type structure, *P6₃/mmc*; NM MnP (Fe VI), non-magnetic MnP-type structure, *Pnma*; *Pmmn* (Fe VII), non-magnetic *Pmmn* structure, *Pmmn*.

According to previous experimental studies and the present calculations, the schematic phase diagram of FeS phases can be proposed (Fig. 8). We propose that the transition sequence of FeS at 0 K is as follows: troilite (Fe I) → antiferromagnetic MnP phase (Fe II) → monoclinic phase (Fe III) → non-magnetic MnP phase (Fe VI) → *Pmmn* phase (Fe VII). However, three other phases (Liquid, Fe IV, and Fe V) were confirmed at high temperatures by experimental studies (Kavner et al., 2001; Urakawa et al., 2004). FeS V has a simple NiAs-type structure. In contrast, FeS IV shows a hexagonal NiAs-type superstructure. The stabilities of these high-pressure phases were not calculated in our study because our calculations were performed at 0 K. As temperatures in the interior of planets are high enough to stabilize the hexagonal NiAs-type superstructure and the simple NiAs-type structure, the relationship between these phases and the non-magnetic MnP-type phase is likely to be of importance in understanding planetary interiors. This is important, especially for Mars, since the transition pressure corresponds to conditions of the Martian core. As the *Pmmn* phase is predicted to be stable at pressures spanning those of the Earth's core (from 130 GPa to >400 GPa), an experimental investigation is needed to confirm this prediction. The existence of this phase and the determination of its properties could shed new light on the properties and evolution of the Earth's inner core.

Acknowledgements

This work made use of the UCL research computing facilities and of HPCx, the UK's national high-performance computing service at the Daresbury Laboratory. Evolutionary crystal structure prediction simulations were performed on computing facilities of ETH Zurich, CSCS (Manno) and Joint Supercomputer Centre of Russian Academy of Sciences (Moscow). The synchrotron radiation experiments were performed at the PF, KEK (Proposal No. 2005G122). This work was supported by NERC Computational Mineral Physic Consortium, UK and Grant-in-Aid for Scientific Research from the Ministry of Education, Culture, Sports, Science and Technology, Japan. ARO gratefully acknowledges grants from the Swiss National Science Foundation (grant 200021-111847/1) and ETH Research Equipment Programme.

References

- Alfè, D., Gillan, M.J., 1998. First principles simulations of liquid Fe–S under Earth's core conditions. *Phys. Rev. B* 58, 8248–8256.
- Alfredsson, M., Price, G.D., Catlow, C.R.A., Parker, S.C., Orlando, R., Brodholt, J.P., 2004. Electronic structure of the antiferromagnetic B1-structure FeO. *Phys. Rev. B* 70, 165111.
- Allègre, C., Manhès, G., Lewin, É., 2001. Chemical composition of the Earth and the volatility control on planetary genetics. *Earth Planet. Sci. Lett.* 185, 49–69.
- Birch, F., 1952. Elasticity and constitution of the Earth's interior. *J. Geophys. Res.* 57, 227–286.
- Blöchl, P.E., 1994. Projector augmented-wave method. *Phys. Rev. B* 50, 17953–17979.
- Dewaele, A., Loubeyre, P., Occelli, F., Mezouar, M., Dorogokupets, P.I., Torrent, M., 2006. Quasihydrostatic equation of state of iron above 2 Mbar. *Phys. Rev. Lett.* 97, 215504.
- Dobson, D.P., Vočadlo, L., Wood, I.G., 2002. A new high-pressure phase of FeSi. *Am. Mineral.* 87, 784–787.
- Dreibus, G., Palme, H., 1996. Cosmochemical constraints on the sulfur content in the Earth's core. *Geochem. Cosmochim. Acta* 60, 1125–1130.
- Fei, Y., Prewitt, C.T., Mao, H.K., Bertka, C.M., 1995. Structure and density of FeS at high pressure and high temperature and the internal structure of Mars. *Science* 268, 1892–1894.
- Gillan, M.J., Alfè, D., Brodholt, J.P., Vočadlo, L., Price, G.D., 2006. First-principles modeling of Earth and planetary materials at high pressures and temperatures. *Rep. Prog. Phys.* 69, 2365–2441.
- Glass, C.W., Oganov, A.R., Hansen, N., 2006. USPEX – evolutionary crystal structure prediction. *Comp. Phys. Comm.* 175, 713–720.
- Gramsch, S.A., Cohen, R.E., Savrasov, S.Y., 2003. Structure, metal-insulator transitions, and magnetic properties of FeO at high pressures. *Am. Mineral.* 88, 257–261.
- Isaak, D.G., Cohen, R.E., Mehl, M.J., Singh, D.J., 1993. Phase stability of wüstite at high pressure from first-principles linearized augmented plane-wave calculations. *Phys. Rev. B* 47, 7720–7731.
- Kavner, A., Duffy, T.S., Shen, G., 2001. Phase stability and density of FeS at high pressures and temperatures: implications for the interior structure of Mars. *Earth Planet. Sci. Lett.* 185, 25–33.
- King, H.E., Prewitt, C.T., 1982. High-pressure and high-temperature polymorphism of iron sulfide (FeS). *Acta Cryst. B* 38, 1877–1887.
- Kobayashi, H., Sato, M., Kamimura, T., Sakai, M., Onodera, H., Kuroda, N., Yamaguchi, Y., 1997. The effect of pressure on the electronic states of FeS and Fe₇S₈ studied by Mössbauer spectroscopy. *J. Phys. Condes. Matter* 9, 515–527.

- Kobayashi, H., Kamimura, T., Alfè, D., Sturhahn, W., Zhao, J., Alp, E.E., 2004. Phonon density of states and compression behavior in iron sulfide under pressure. *Phys. Rev. Lett.* 93, 195503.
- Kresse, G., Furthmüller, J., 1996. Efficient iterative schemes for *ab initio* total-energy calculations using a plane-wave basis set. *Phys. Rev. B* 54, 11169–11186.
- Kresse, G., Joubert, D., 1999. From ultrasoft pseudopotentials to the projector augmented-wave method. *Phys. Rev. B* 59, 1758–1775.
- Kusaba, K., Syono, Y., Kikegawa, T., Shimomura, O., 1997. Structure of FeS under high pressure. *J. Phys. Chem. Solids* 58, 241–246.
- Kusaba, K., Syono, Y., Kikegawa, T., Shimomura, O., 1998. High pressure and temperature behavior of FeS. *J. Phys. Chem. Solids* 59, 945–950.
- Larson, A.C., von Dreele, R.B., 2000. General Structure Analysis System (GSAS). Los Alamos National Laboratory Report LAUR, pp. 86–748.
- Marshall, W.G., Nelmel, R.J., Loveday, J.S., Klotz, S., Besson, J.M., Hamel, G., Parise, J.B., 2000. High-pressure neutron-diffraction study of FeS. *Phys. Rev. B* 61, 11201–11204.
- Martin, P., Price, G.D., Vočadlo, L., 2001. An *ab initio* study of the relative stabilities and equations of state of FeS polymorphs. *Mineral. Mag.* 65, 181–191.
- Methfessel, M., Paxton, A.T., 1989. High-precision sampling for Brillouin-zone integration in metals. *Phys. Rev. B* 40, 3616–3621.
- Nelmel, R.J., McMahon, M.I., Belmonte, S.A., Parise, J.B., 1999. Structure of the high-pressure phase III of iron sulfide. *Phys. Rev. B* 59, 9048–9052.
- Oganov, A.R., Glass, C.W., 2006. Crystal structure prediction using evolutionary techniques: principles and applications. *J. Chem. Phys.* 124, 244704.
- Oganov, A.R., Glass, C.W., Ono, S., 2006. High-pressure phases of CaCO₃: crystal structure prediction and experiment. *Earth Planet. Sci. Lett.* 241, 95–103.
- Ohfuji, H., Sato, N., Kobayashi, H., Ohishi, Y., Hirose, K., Irifune, T., 2007. A new high-pressure and high-temperature polymorph of FeS. *Phys. Chem. Minerals* 34, 335–343.
- Ono, S., Kikegawa, T., 2006. High-pressure study of FeS, between 20 and 120 GPa, using synchrotron X-ray powder diffraction. *Am. Mineral.* 91, 1941–1944.
- Ono, S., Ohishi, Y., Kikegawa, T., 2007a. High-pressure study of rhombohedral iron oxide, FeO, at pressures between 41 and 142 GPa. *J. Phys. Condens. Matter* 19, 036205.
- Ono, S., Kikegawa, T., Ohishi, Y., 2007b. Equation of state of the high-pressure polymorph of FeSi to 67 GPa. *Eur. J. Mineral.* 19, 183–187.
- Perdew, J.P., Burke, K., Ernzerhof, M., 1996. Generalized gradient approximation made simple. *Phys. Rev. Lett.* 77, 3865–3868.
- Rueff, J.P., Kao, C.C., Struzhkin, V.V., Badro, J., Shu, J., Hemley, R.J., Mao, H.K., 1999. Pressure-induced high-spin to low-spin transition in FeS evidenced by X-ray emission spectroscopy. *Phys. Rev. Lett.* 82, 3284–3287.
- Sherman, D.M., 1995. Stability of possible Fe–FeS and Fe–FeO alloy phases at high pressure and the composition of the Earth's core. *Earth Planet. Sci. Lett.* 132, 87–98.
- Takele, S., Hearne, G.R., 1999. Electrical transport, magnetism, and spin-state configurations of high-pressure phases of FeS. *Phys. Rev. B* 60, 4401–4403.
- Toby, B.H., 2001. EXPGUI, a graphical user interface for GSAS. *J. Appl. Cryst.* 34, 210–221.
- Tremel, W., Hoffmann, R., Silvestre, J., 1986. Transitions between NiAs and MnP type phases: and electronically driven distortion of triangular (3⁶) nets. *J. Am. Chem. Soc.* 108, 5174–5187.
- Urakawa, S., Someya, K., Terasaki, H., Katsura, T., Yokoshi, S., Funakoshi, K., Utsumi, W., Katayama, Y., Sueda, Y., Irifune, T., 2004. Phase relations and equations of state for FeS at high pressures and temperatures and implications for the internal structure of Mars. *Phys. Earth Planet. Inter.* 143–144, 469–479.
- Valle, M., 2005. STM3: a chemistry visualization platform. *Z. Krist.* 220, 585–588.
- Vočadlo, L., Price, G.D., Wood, I.G., 1999. Crystal structure, compressibility and possible phase transition in ϵ -FeSi studies by first-principles pseudopotential calculations. *Acta Cryst. B* 55, 484–493.
- Vočadlo, L., Alfè, D., Gillan, M.J., Price, G.D., 2000. First principles calculations on the diffusivity and viscosity of liquid Fe–S at experimentally accessible conditions. *Phys. Earth Planet. Inter.* 120, 145–152.
- Vosko, S.H., Wilk, L., Nusair, M., 1980. Accurate spin-dependent electron liquid correlation energies for local spin density calculations: a critical analysis. *J. Phys.* 58, 1200–1211.
- Wang, Y., Perdew, J.P., 1991. Correlation hole of the spin-polarized electron gas, with exact small-wave-vector and high-density scaling. *Phys. Rev. B* 44, 13298–13307.